AIAA-2003-1014

Soot Concentration and Velocity Measurement in an Acoustic Burner

Ping Yang and Jerry M. Seitzman
Georgia Institute of Technology
Atlanta, GA

41th Aerospace Sciences
Meeting & Exhibit
January 6-9, 2003 / Reno, NV

Soot Concentration and Velocity Measurement in an Acoustic Burner

Ping Yang* and Jerry M. Seitzman†

Georgia Institute of Technology
Aerospace Combustion Laboratory
School of Aerospace Engineering
Atlanta, GA 30332-0150

Abstract

Laser Induced Incandescence (LII) and Particle Vaporization Velocimetry (PVV) were used to measure soot concentration and velocity in an acoustically excited combustion chamber. This acoustic burner provides a controllable environment for the study of soot formation and destruction in an unsteady flow relevant to turbulent combustion. Results are presented for a nonpremixed jet of acetylene in a coflow of air at two fuel flow rates. One condition is a laminar jet; the other corresponds to a transitional case. The acoustic forcing is shown to produce vortices that enhance entrainment and fuel-air mixing. In both jets, the acoustic forcing decreases the total amount of soot in the combustor compared to the corresponding unforced jet. However, the forcing only slightly decreases the upper range of soot concentrations present in the flame. In addition, luminosity measurements show that the average soot temperature is increased when the combustor is acoustically excited.

Introduction

Combustion-generated soot, in particular, fine soot particles (less than a few μm) are of great concern because of their ability to penetrate not only into indoor areas but to the depths of the respiratory system[1]. They can lead to severe problems for human health, increasing risk of cancer and many other diseases. Soot may also cause environmental effects at higher altitudes. It is suspected to be a key player in the "greenhouse" warming effect, due to its influence on solar radiation and cloud formation, from the increased number of cloud-condensing nuclei.[2] Soot has engineering implications as well. Soot is often the dominant source of flame radiation and influences local flame temperatures and combustor wall and liner temperatures.

Most current soot research is interested in trying to understand the processes by which soot is created and destroyed in and around flames. In addition, soot is also an indicator of incomplete combustion and soot measurements have been used for active control strategies.[3,4,5]

The use of steady flames is very popular in soot formation research, and there is a large body of experimental data used to understand soot initiation, growth and destruction in steady, laminar flames. Attempts have also been made to study soot formation and evolution in unsteady laminar flames. In previous experiments,[6,7] a pulsed fuel jet was used to generate unsteady flames. That work showed that unsteady flames, while not turbulent, can be an effective approach for soot formation research targeted towards turbulent combustion.

Laser-induced incandescence (LII) is a powerful technique that has been demonstrated for volume fraction measurements of flames,[8,9] engines,[10] and exhaust flows.[11] Soot particles are comprised of branchy aggregates of nominally spherical primary particles of graphitic-like carbon on the order of a few tens of nanometers in diameter. LII is based on exposing these small soot particles to a high power laser. The soot particles absorb laser energy and are rapidly heated, and their incandescence increases. If the laser fluence of a pulsed laser is sufficiently high, a particle approaches it vaporization temperature (around 3900 K for graphite), and vaporization becomes the dominant heat loss mechanism. Further increases in temperature are balanced by large increases in vaporization rate.

In a previous paper, we introduced a velocity measurement technique, Particle Vaporization Velocimetry (PVV),[12] which is related to LII. This approach is based on flow tagging velocimetry.[13,14] In PVV, a high power laser is used to vaporize a soot containing region, which is then monitored at a later time using either LII or scattering. A system designed for LII imaging can easily be adapted for velocity measurements and even simultaneous LII-PVV measurements, for example to produce local soot flux measurements. Thus these approaches have potential applications in soot containing flows such as open flames, gas turbine combustors, and automotive engines. In this paper, we report on application of these techniques to the study of soot in unsteady,

* Research Assistant, Student Member AIAA
† Associate Prof., Associate Fellow AIAA

nonpremixed flames, forced by acoustic excitation in an atmospheric pressure, combustion chamber.

Experimental Procedure

Acoustic Burner

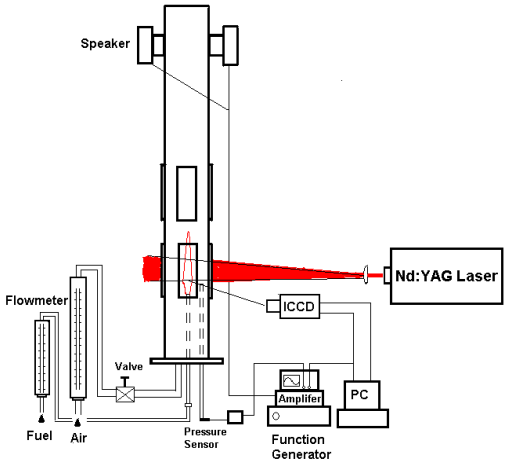

Figure 1. Schematic of acoustic burner, including electronics to generate acoustic waves, laser system for soot measurements, and detectors.

The PVV technique and soot concentration measurement have been extended to an "acoustic burner"(Figure1). Acetylene (C_2H_2) chosen for its high sooting tendency flows through a stainless steel tube of 0.8 mm i.d.. It is surrounded by a flow of air contained in a 9.8 cm square, 120 cm long tube that has two acoustic generators mounted on the top. The acoustic burner is designed as a 5/4 wavelength tuber with a resonant frequency of approximately 320 Hz. The air flowrate for all measurements is fixed at 5690 cm^3/s.

Two flame cases were studied: a laminar and transitional ("unsteady") flow. For the laminar case, the fuel flow rate is 1.67 cm^3/s. In the unsteady case, the flow rate is 10.5 cm^3/s. Both the fuel and air flowrates are measured by calibrated rotameters. There are a total of 8 windows in the square tube, arranged in group of 4 at two heights. Each window is 14.5 cm in height and 4.1 cm in width. The laser beams pass through two facing windows, an ICCD camera images the flame through one of the remaining windows, the last window is used temporally introduce an ignition source. The height of the acoustic burner can be adjusted while the optical systems remain fixed. In one corner of the square tube is a smaller tube, which leads to a pressure sensor for measuring the acoustic pressure. The location of the pressure sensor also can be changed to correspond to the height of the small fuel tube. In our experiments, the flame sits close to the pressure node of the burner, where the acoustic pressure is close to its minimum value and acoustic velocity is near its maximum value. This allows a low input acoustic power from the acoustic generators to efficiently create acoustic velocity fluctuations.

PVV

In our previous research[1] we developed Particle Vaporization Velocimetry (PVV) for 1-d velocity measurements. Here, we extend the technique to 2 dimensions by using multiple laser beams. The marking and readout laser pulses are produced by a dual-head Nd:YAG laser (Continuum Surelite-I PIV). The delay between the two laser pulses can be varied from 0-100 ms, and the lasers (7 ns FWHM) are nominally operated at 10 Hz.

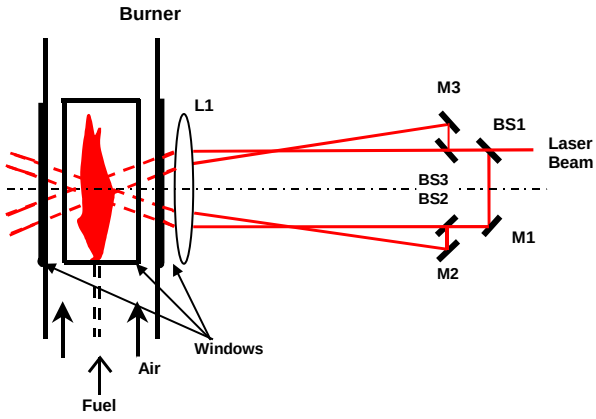

Figure 2. PVV optical setup(marking beam): L1 f=150mm cylindrical lens; mirrors M1, M2, M3; e 50/50 beam splitters BS1, BS2 BS3.

The fundamental (1064 nm) output of one head is used as the marking beam. The maximum pulse energy is 450 mJ. The 8 mm diameter beam (measured by a burn mark method) is separated into four beams, as shown in Figure 2. The result is four similar beams, each ~110 mJ/shot. It is important to make sure the four beams travel inside a single plane and form a "grid" after being focused by a 50×60mm, 150 mm focal length cylindrical lens. Each marking beam thus forms a small sheet, each 8 mm and 0.5 mm (FWHM) thickness. The sheet marks a thin region that extends across a wide path normal to the flow. Results reported here are for average energy fluences 2 J/cm^2, more than 3 times of the IR vaporization threshold (~0.6 J/cm^2).

The visible readout beam is produced by frequency-doubling (532 nm) the output of the second Nd:YAG laser head, with a maximum pulse energy of 200 mJ. The image beam is focused by a 90 mm diameter, 500 mm focal length fused-silica cylindrical lens in the vertical direction and is spread in the horizontal direction by another cylindrical lens with 25 mm focal length. This yields an imaging sheet that is 0.8 mm thick and 75 mm high. The fluence of the

imaging beam is fixed (~0.1 J/cm^2) and just below the vaporization threshold intensity. Thus, it can be used for LII measurements of the soot particles.

The readout sheet is carefully position to coincide with the plane defined by the four crossing points of the marking beams. The readout sheet is also carefully aligned to be normal to each of the marking sheet. The image is recorded at a right angle to the laser beam by an intensified CCD camera (Princeton Instruments). In most experiments, the CCD camera exposure starts with the onset of the green laser, and lasts 50 ns.

LII

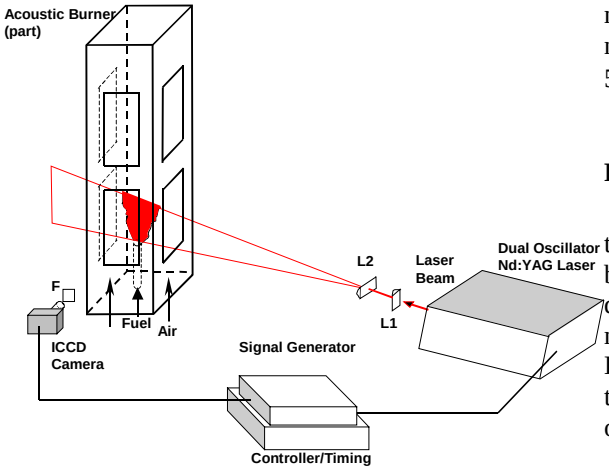

Figure 3. LII optical setupL1 f=500mm cylindrical lens; L2: f=250mm cylindrical lens BS3.

Two-dimensional soot concentration fields are measured with the LII technique. The IR YAG beam is focused by a 500 mm focal length, cylindrical lens in the horizontal direction and spread vertically by a 250 mm focal length cylindrical lens. This yields a laser sheet that is ~0.08 mm thick and 45 mm high with the thickness parallel to the flow direction. The fluence of the imaging beam is fixed for all measurements at ~0.75 J/cm^2, which is sufficient to produce quantitative LII signal of soot generated by the flame. All images are recorded at roughly 90° to the propagation direction of the IR laser sheet by the ICCD camera. The LII signals are recorded with a 50ns gate, camera lens aperture set to f/2.8, and sometimes, a ND (neutral density) 1 filter in front of the lens.

In order to get quantitative soot concentrations, system calibration is necessary. An ethylene laminar flame burner was chosen as the soot concentration standard, because there is large amount experimental data available. Here the calibration data were based on Quay, *et al.*[15] and Greenberg and Ku.[16] During calibration process, the LII system was kept exactly same as in the experiment, the acoustic burner was simply replaced with the laminar flame burner.

Soot Luminosity

Measurements of natural soot luminosity were also recorded with the ICCD camera (no laser). Broadband radiation, as well as narrowband blue and red wavelength measurements were recorded. For the broadband measurements, the ICCD gating time was 500 ns, the lens aperture setting was f/2.8, and no filtering was applied. The blue wavelength measurement was achieved by placing a 430 nm, 10 nm FWHM bandpass filter (CVI, 50×50×2 mm) in front of the ICCD camera. The peak transmissivity was 50%. Similarly, the red measurements were acquired with a 650 nm, 10 nm FWHM bandpass filter (CVI, 50×50×2 mm), with 77% maximum transmission. In both narrowband cases, the ICCD gate time was increased to 5 μs to compensate for the weaker narrowband signals.

Results and Discussion

PVV Velocity Measurements

Figure 4 shows three instantaneous LII images of the unsteady case at 200μs delay after the marking beam. Both unforced flame and forced flames (at different acoustic phases) are included. The four marking beams form a diamond-like "grid" (4x12mm). Due to the limited soot extent in the small flame, part of the "grid" is typically out of the soot field, and only part of the grid is visible.

For the unforced flame, the marked region stays nearly straight; the burned holes in the soot field primarily translate upward indicating the velocity field is essentially axial. This is much different from the forced flame results, which show the marked lines become highly curved. This suggests the axial velocity is change rapidly across the region. Qualitatively, the velocity images suggest the presence of a vortex ring, which is also indicated by the shape of the soot region. At the 96° phase, the four marked lines move slightly to the right, while for the 168° case, they move significantly left. Thus there is also a greater radial velocity fluctuation when forcing is applied.

Quantitative, two-dimensional velocities can be determined by measurement of the displacement of the intersection points over the known delay. While shorter time delays provide better instantaneous velocity results, it can become hard to accurately determine small displacements due to the finite size of the ICCD pixels. In this experiment, a 100μs delay was chosen because it is long enough to achieve good image resolution (more than 6 pixels generally), but still short enough to obtain reasonable instantaneous measurements.

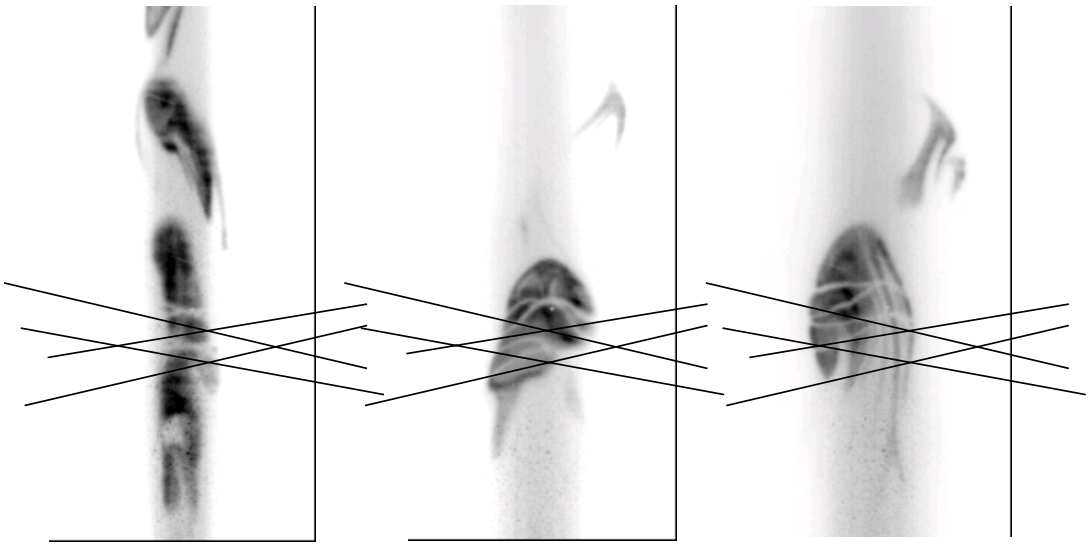

Figure 4. LII images (the gray scale is inverted) at 200μs delay after the IR marking laser: (a)unforced flame, (b) forced beam at 96ºphase, (c) 168º. Real image size is 47.3mm high by 23.7mm wide. The location of the marking beams is indicated by the thin lines.

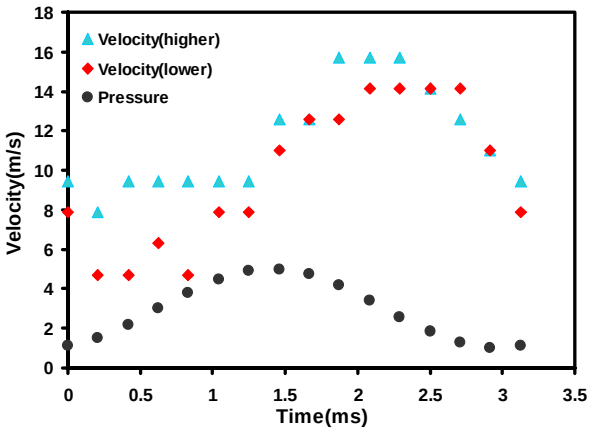

Figure 5. Average axial (vertical) velocity components of the based on 100 frame average with 100μs delay relative to the marking laser.

Figure 5 shows axial velocity data corresponding to different phases of the acoustic phase. Also shown is the acoustic pressure. The data have been adjusted to account for electronic propagation delays and acoustic delays in the sensor tube. In general, the velocity fluctuation appears to be nearly 90° out-of-phase with the pressure fluctuation, as is expected for an acoustic velocity.

Two velocity locations are shown, one for the upper intersection point and one for the lower. The velocity at the upper point varies between 8 and 16m/s, while the lower point's velocity is between 4.3 and 14m/s. The average velocity for the combined data is ~11 m/s, about the same as the average velocity measured without acoustic forcing. Therefore, the velocity fluctuation is roughly ±5 m/s due to forcing.

This fluctuation can be compared to an acoustic velocity fluctuation based on the measured acoustic pressure. This relationship is given by

$$v_{acoustic} = p_{acoustic} / \rho c$$

where the acoustic velocity and pressure are based on the maximum locations, ρ is the density and c is the speed of sound. It is reasonable to use the unburned air density and speed of sound to estimate the acoustic velocity level, since most of the gas in the burner is cold air.

Based on the measured acoustic pressure at the pressure antinode, the acoustic velocity fluctuation we would expect to see in the flame region is ±4.2 m/s. This calculated acoustic velocity fluctuation is similar to that measured by PVV in the burner. The higher measured value may be due to increased heat release in the soot region caused by enhanced fuel-air mixing. The hotter gases would expand and increase the fluctuating velocity.

As seen in Figure 5, the upper and lower intersections have different measured velocities at most phases. Generally, the upper point has the higher velocity. As noted previously, the soot velocity points seem to be located near the axis of a vortex ring. These structures entrain oxidizer and enhance the fuel-air mixing. The enhanced mixing of fuel and air entering the bottom of the ring, may lead to enhanced combustion and heat release. Therefore, the upper intersection point may be hotter and have a higher velocity.

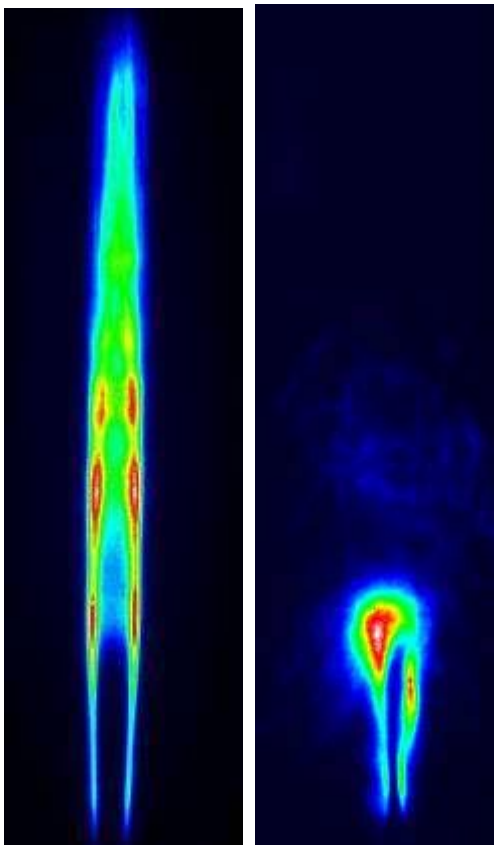

(a) (b)

Figure 6. Flame LII images (53.7×13.7mm) from the a)unforced and b) forced laminar flames, but with the intensity scale expanded by a factor of 2 for the forced case. Both images represent 100 frame averages**.**

LII Concentration Measurements

LII-based soot concentration measurements were obtained under both acoustically forced and unforced conditions. The fundamental wavelength of the Nd:YAG laser (IR, 1064nm) was chosen for the concentration measurements because of its long wavelength (compared to the green, second harmonic output). LII soot concentration measurements are generally more accurate if the sizes of the particles are much smaller than the laser wavelength. In this case, the LII signals are nearly linearly proportional to the volumetric concentration (or volume fraction) of soot inside the flame. In addition, the ICCD camera is not sensitive to the IR scattering from the soot particles. Thus this interference can be removed without the need for adding wavelength filters that also result in some loss in signal.

Figure 6 shows average LII soot images from the laminar flame for both unforced and forced conditions. Since the same gray scale in the unforced case represents about twice the soot concentration as in the forced case, one can see that the peak (average) soot concentrations in the forced case are lower. Also due to the much larger spatial extent of the soot field in the unforced case, it has a much greater spatially integrated concentration, i.e., total soot mass or soot volume, than the forced flame. Based on the average images, the forced and unforced flames are roughly axisymmetric (again, only on average). Also, the IR laser sheet passes through the axis of the flame. Therefore, the volumetrically integrated LII signal can be calculated by rotating the LII imaging sheet 360 degree around the flame axis. Based on this approach, the volumetrically integrated soot mass for the unforced flame is calculated to be four times larger than that of the forced flame.

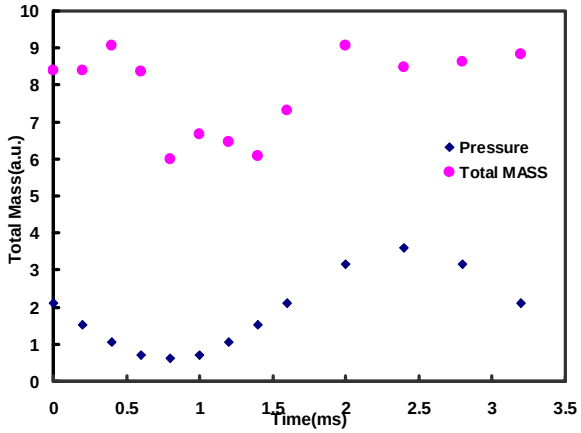

Figure 7. Total soot mass as function of time within an average forcing cycle for forced "laminar" case. The middle of the flame is located 75mm above the pressure minimum. Acoustic pressure also shown for reference.

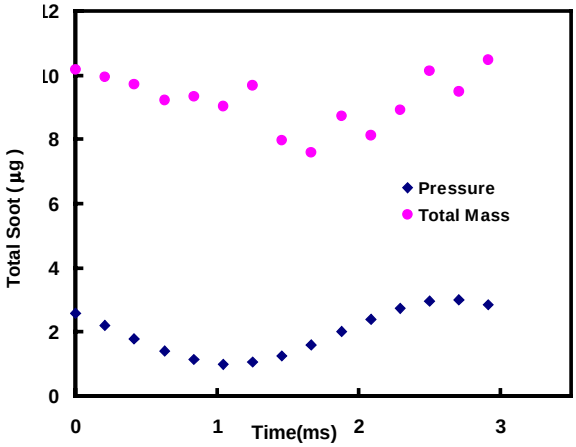

Figure 8. Total soot volume/mass as function of time within an average forcing cycle for forced "unsteady" case. The middle of the flame is located 75mm above the pressure minimum.

Of course, the soot field varies with time, especially for the forced case where it is primarily a function of the phase of the forcing signal, e.g., the acoustic pressure. Figure 7 shows the integrated LII signal level as a function of phase, again for the laminar flame case. Because the laminar average data was acquired with a different camera then all the rest of the measurements presented here, the soot values are not absolute. Figure 8 shows the results for the "unsteady" flame (now absolute values). Similar to the laminar case, the spatially integrated soot mass for the acoustically forced case is lower on average than the unforced case (~10 μg forced compared to ~30 μg unforced).

As illustrated by these results, the total amount of soot inside the forced flame is decreased compared to the unforced flame. The applied acoustic field energy generates velocity fluctuations, which act to create vortices in the flame, thereby enhancing the entrainment of the ambient air to the fuel area. This enhances the mixing rate in the flame, reduces its extent, and decreases the total amount of soot inside the flame.

In both the laminar and unsteady cases, the soot is seen to decline the most during the time when the acoustic pressure has passed its minimum value and is rising towards its maximum. This range of phases corresponds to the time when the acoustic velocity in the region of the flame induces a (relative) upwards flow in the surrounding air. This in turn would increase the mixing of the flame gases with the surrounding cooler air. A decrease in the **total** soot volume can be caused either by increased oxidation of the soot or reduced production (but not by dilution). With the increase in mixing with air, it is likely that the rate of soot oxidation is enhanced during this time.

The results presented in Figures 7 and 8 are based on spatially integrated, and time- (or phase-) averaged LII measurements. It is also instructive to examine other statistical aspects of the data. Therefore, probability density function (PDFs) of the LII measurements were also calculated for the data sets. The distribution function evaluated at a given soot volume fraction, f, represents the (normalized) fraction of all pixels in a data set that have a soot volume fraction that is between f and $f+df$. Each data set is composed of the pixels in a defined region of each 2-d image, and in all the images acquired that correspond to the same nominal conditions. For example, a data set consisting of 50 images and a 200×400 pixel region would be composed of 4 million data points. The normalization produces a distribution function with the following property,

$$\int_0^\infty PDF(f)df = 1 \cdot \qquad (1)$$

Conditional PDFs were also calculated. In this case, the pixels included in the PDF calculation were conditioned on whether they contained soot, i.e., pixels that did not contain measurable levels of soot were discarded from the sample. In the current experiments, there was a measurable amount of luminosity (incandescence) from the flame heated soot in the region in front and behind the laser sheet during the 50ns gate of the camera. While averaged measurements of the natural soot luminosity were used to remove this interference from the averaged LII data presented above, they cannot be used to correct the instantaneous results. From regions located above and below the laser sheet in the LII images, it was found that 98% of the luminosity signals would correspond to LII signals from soot volume fractions below 4 ppm. Therefore, this value was chosen as the threshold to condition the data sets. This value was also chosen as the minimum value to present in the graphs below.

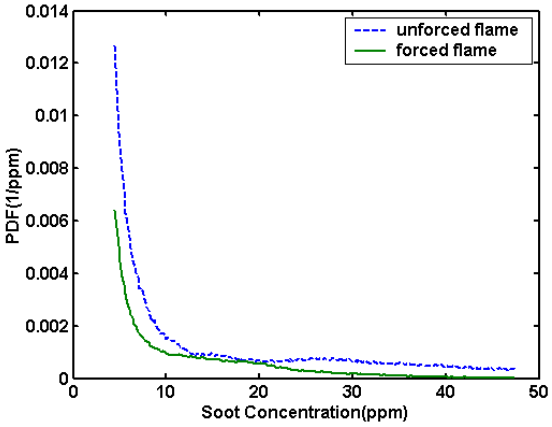

Figure 9. Probability distribution for acoustically forced and unforced laminar flame.

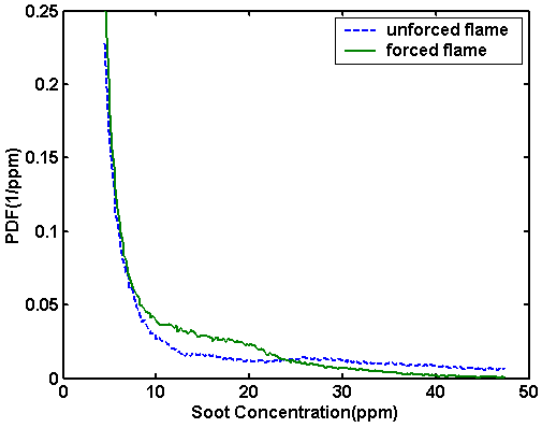

Figure 10. Conditional probability distribution for acoustically forced and unforced laminar flame.

Figures 9 and 10 show the standard and conditioned PDF for the laminar case data, unforced and forced (at one typical phase of the excitation). Both versions of the PDF clearly show that the general range of soot concentrations found in the forced flame is similar to that of the unforced case. The unconditioned PDF (Figure 9) indicates a decrease in the distribution for all soot concentrations when forcing is applied. However, the conditioned PDF (Figure 10) shows that for instances *when soot is present*, there is a shift in the distribution from higher to lower values. Thus it is clear that the lower averaged results presented above for the forced flame are due to periods where there is no soot present at a pixel. Also in both the forced and unforced cases, there is a rapid drop off in the PDF from ~4 to 9 ppm; the most probable soot concentration occurs at some relatively low value – likely diluted soot away from the active flame region.

In the unforced case, there is a "plateau" region in the PDF above ~12 ppm; the PDF is nearly flat there. While not shown in the figure, the PDF does descend towards zero for soot concentrations near 70 ppm. The forced case PDF is somewhat different. Instead of the flat plateau, it exhibits a slow decline over the range 10-40 ppm. Essentially, the forcing seems to increase the likelihood of soot in the range 10-25 ppm, and lower it for values above 25 ppm. Overall, the forcing decreases the total amount of soot in the burner, as well as the peak instantaneous soot concentrations.

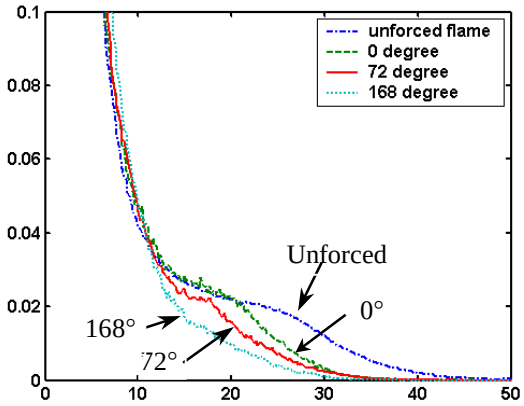

Figure 11. Conditional PDFs for unsteady flame, unforced and forced flame (at 3 phase angles).

Figure 11 shows the conditional PDF results for the unsteady case. As in the laminar results, the unconditioned PDFs (not shown here) would simply illustrate that a larger fraction of the combustor contains soot when the flame is not forced. Figure 11 shows forced case PDFs at three of the 16 different phases measured: 0º, 72º, 168º. The range of soot concentrations in all cases (unforced and forced) is generally similar to that found in the forced laminar results. For the unforced condition, the shape of the unsteady flame PDF is similar to that of the forced laminar condition. After an initial rapid decrease in the PDF at low concentrations (~4-10 ppm), there is a gradual decline in the PDF above ~10ppm. The most possible reason for the similarity is that the unforced, unsteady flame already contains sufficient vorticity that convective mixing between fuel and air is enhanced.

Like the laminar case, forcing decreases the peak volume fraction. For the unsteady case, the decrease is from 45 ppm for the unforced case, to ~30 ppm with forcing, with the result somewhat dependent on phase. The largest drop in the high soot concentrations occurs at the 168° phase angle. This corresponds to the same region (90-180°) where the total soot mass decreased the most (see Figure 8). From individual instantaneous images (not shown), the soot field does change with phase. The soot field is a single structure at 0°, but stretches out gradually until the high soot concentration region eventually breaks into two or more pieces. As indicated before, the acoustic velocity fluctuations are likely the key. At 0°, the acoustic velocity has reached its maximum downward value and the flame appears flat and short. But when the acoustic velocity has reached its maximum upward value (135°), the flame has been stretched out and eventually breaks.

Luminosity Measurements

Part of the original motivation for this work was observations in acoustically excited incinerators that soot exhausts dropped, but radiation levels increased. Therefore in addition to the LII measurements, the natural (laser off) soot luminosity was measured using the same detection system. Both broadband luminosity results, integrated over the complete sensitivity range of the camera system (~400-650nm), and narrowband results at 650nm and 430nm were acquired.

Figure 12 presents the spatially integrated, broadband luminosity results for the laminar case. Overall, the luminosity signal of the forced case is much higher than that of the unforced case, around 4.5 times. This is despite the fact that the total amount of soot drops by 4 times when forcing is applied. Therefore on average, each gram of soot in the forced flame must produce 18 times more radiation (weighted by the camera sensitivity) than in the unforced case. This would suggest the average soot temperature in the forced case must be noticeably higher than for the unforced laminar flame. The narrowband luminosity measurements agree. On average, the ratio of radiation at 430 nm to that at 650 nm increased by a factor of ~3 when forcing was applied. The relative increase in the blue spectrum indicates the soot was indeed hotter.

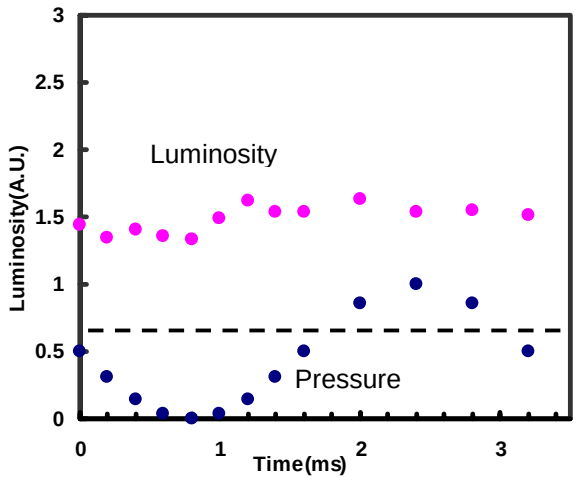

Figure 12. Integrated (natural) soot luminosity for forced laminar flame over an average cycle (also shown is acoustic pressure variation). The unforced, average, laminar flame luminosity is indicated by the dashed line.

This means that either the flame temperatures are much higher in the forced case, or a much larger fraction of the soot exists in the high temperature region of the flame. In any case, this would be associated with the improved fuel-air mixing produced by the unsteady (forced) flowfield. Figure 10 also indicates that the soot luminosity (on average) is not a strong function of the forcing phase angle. There does appear to be a small decrease in the broadband luminosity while the acoustic pressure is approaching its minimum value (0-90°). This would correspond to times when the acoustic velocity is downward.

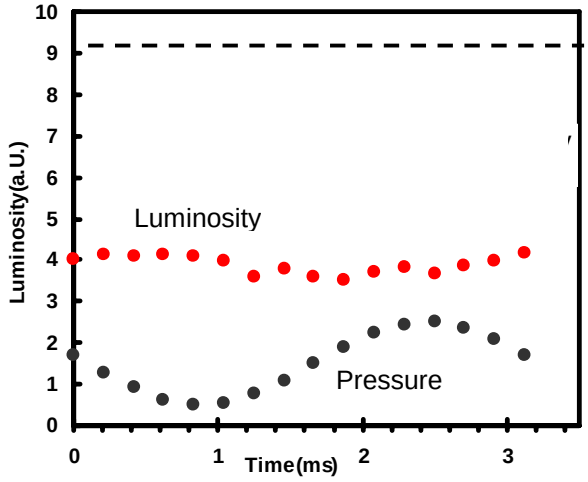

Figure 13. Integrated (natural) soot luminosity for forced unsteady flame over an average cycle (also shown is acoustic pressure variation). The average, unforced, flame luminosity is indicated by the dashed line.

Figure 13 shows that the unsteady flame has higher luminosity than the laminar flame (forced or unforced). Again, this follows from the fact that it is consuming fuel at a higher rate. Unlike the laminar case, the acoustic forcing decreases the broadband luminosity almost to one half. However, the decrease in luminosity is less than 2.5 times, the decrease in total amount of soot (2.9 times). Therefore, the soot must again have a higher average temperature in the forced case. Like the laminar case, the dependence of the luminosity on phase is small (<15%), however the minimum luminosity now occurs in the range 90-270°. This generally follows the variation in total soot mass seen in Figure 6.

Summary

LII concentration and PVV velocity measurements have been successfully applied in an acoustically excited combustor. This is the first demonstration of two-dimensional velocity measurements using PVV. The measured velocity fluctuations are close to the values predicted for the acoustic velocity, based on the measured acoustic pressures. The velocity measurements, combined with simultaneous LII images, indicate that the acoustic forcing creates vortices that contain a large fraction of the soot.

The LII-based concentration results show that for both the laminar and unsteady jet flames (based on unforced velocities), the total amount of soot was decreased by acoustic forcing. Not only does the forcing decrease the size of the flame (and decrease the soot containing volume), the conditional pdf results also show that it reduces the peak soot concentrations seen in the flame. The enhanced entrainment of air into the fuel region is the likely source of the reduced soot levels. Not only does the fuel have less time to pyrolyze, the rapid infusion of oxidizer can destroy the soot that is produced. Work is underway to combine the PVV and LII soot measurements into a measurement of local soot flux.

Finally, radiation measurements of the natural soot luminosity indicate the average soot temperature increases when forcing is applied. So even though the forced flames produce less soot, the soot radiation can actually increase.

Acknowledgements

The authors gratefully acknowledge the help of D. Scarborough and Y. Jang in development of the acoustic burner.

References

[1]Wilson, R. and Spengler, J. (Ed.), *Particles in Our Air*, Harvard University Press, 1996 p.41-62.

[2]Klingenberg, H., *Automobile Exhaust Emission Testing: Measurement of Regulated and Unregulated Exhaust Gas Components, Exhaust Emission Tests*, Springer Series in Environmental Engineering, Springer-Verlag, New York, 103-119 (1996).

[3]Brouwer, J., Ault, B. A., Bobrow, J. E., and Samuelsen, G. S., "Active Control Application to a Model Gas Turbine Combustor," ASME Conference Paper 90-GT-326, Gas Turbine and Aeroengine Congress and Exposition, Brussels, Belgium (1990).

[4]Burtscher, H., Schmidt-Ott, A., and Siegmann, H. C., "Monitoring Particulate Emissions from Combustions by Photoemissions", *Aerosol Sci. and Tech.* **8**, 125-132 (1988).

[5]Hartman, P. G., Plee, S. L., and Bennethum, J. F., "Diesel Smoke Measurement and Control Using an In-cylinder Optical Sensor", *SAE Transactions*, Vol. 100, Sect. 3, 1259-1272 (1991).

[6]Christopher R Shaddix, Kermit C. Smyth "Laser Induced Incandescence Measurements of Soot Production in Steady and Flickering Methane, Propane and Ethylene Diffusion Flames" Combustion and Flame 107:418-452(1996)

[7]Kermit C. Smyth and Joel. E. Harrington, "Greatly Enhanced Soot Scattering in Flickering CH_4/Air Diffusion Flames," Combustion and Flame 95:229-239(1993)

[8]Vander Wal, R. L. and Weiland, K. J., "Laser-Induced Incandescence: Development and Characterization Towards a Measurement of Soot Volume Fraction," *Appl. Phys. B,*. **59**, 445-452 (1994).

[9]Shaddix, C., and Smyth, K., "Laser-Induced Incandescence Measurements of Soot Production in Steady and Flickering Methane, Propane, and Ethylene Diffusion Flames," *Combust. and Flame* **107**, 418-452 (1996).

[10]Dec, J. E., zur Loye, A. O., and Siebers, D. L., "Soot Distribution in a D.I. Diesel Engine Using 2-D Laser-Induced Incandescence," SAE Paper 910224 (1991).

[11]R. T. Wainner and J. M. Seitzman, "Soot Measurements in a Simulated Engine Exhaust using Laser-Induced Incandescence," AIAA Journal, Vol.37 738-743(1999).

[12]P. Yang and J.M.Seitzman "Particle Vaporization Velocimetry For Soot–containing Flows" AIAA-2000-0645, Reno, NV, January, 2000 .

[13]R. W. Pitz, T. M. Brown, S. P. Nandula, P. A. Skaggs, P. A. DeBarber, and M. S. Brown, "Unseeded Velocity Measurement by Ozone Tagging Velocimetry," Optics Letters **21**, 755-757 (1996).

[14]B. Stier and M. M. Koochesfahani, "Molecular Tagging Velocimetry (MTV) Measurements in Gas Phase Flows," Experiments in Fluids **26**, 297-304 (1999).

[15]Quay, B., Lee, T. W., Ni, T., and Santoro, R. J., .Spatially Resolved Measurements of Soot Volume Fraction Using Laser-Induced Incandescence,. *Combust. and Flame*, Vol. 97, 1994, p. 384-392.

[16]Greenberg, P. S. and Ku, J. C., .Soot Volume Fraction Imaging,. *Applied Optics*, Vol. 36, No. 22, August, 1997, p. 5514-5522.